Rotavirus Disrupts Calcium Homeostasis by NSP4 Viroporin Activity

Joseph M. Hyser,[a] Matthew R. Collinson-Pautz,[a,b] Budi Utama,[a] and Mary K. Estes[a]

Department of Molecular Virology and Microbiology, Baylor College of Medicine, Houston, Texas, USA,[a] and Texas Medical Center Summer Research Internship Program, Augustana College, Rock Island, Illinois, USA[b]

ABSTRACT **Many viruses alter intracellular calcium homeostasis. The rotavirus nonstructural protein 4 (NSP4), an endoplasmic reticulum (ER) transmembrane glycoprotein, increases intracellular levels of cytoplasmic Ca^{2+} ($[Ca^{2+}]$cyto) through a phospholipase C-independent pathway, which is required for virus replication and morphogenesis. However, the NSP4 domain and mechanism that increases $[Ca^{2+}]$cyto are unknown. We identified an NSP4 domain (amino acids [aa] 47 to 90) that inserts into membranes and has structural characteristics of viroporins, a class of small hydrophobic viral proteins that disrupt membrane integrity and ion homeostasis to facilitate virus entry, assembly, or release. Mutational analysis showed that NSP4 viroporin activity was mediated by an amphipathic α-helical domain downstream of a conserved lysine cluster. The lysine cluster directed integral membrane insertion of the viroporin domain and was critical for viroporin activity. In epithelial cells, expression of wild-type NSP4 increased the levels of free cytoplasmic Ca^{2+} by 3.7-fold, but NSP4 viroporin mutants maintained low levels of $[Ca^{2+}]$cyto, were retained in the ER, and failed to form cytoplasmic vesicular structures, called puncta, which surround viral replication and assembly sites in rotavirus-infected cells. When $[Ca^{2+}]$cyto was increased pharmacologically with thapsigargin, viroporin mutants formed puncta, showing that elevation of calcium levels and puncta formation are distinct functions of NSP4 and indicating that NSP4 directly or indirectly responds to elevated cytoplasmic calcium levels. NSP4 viroporin activity establishes the mechanism for NSP4-mediated elevation of $[Ca^{2+}]$cyto, a critical event that regulates rotavirus replication and virion assembly.**

IMPORTANCE **Rotavirus is the leading cause of viral gastroenteritis in children and young animals. Rotavirus infection and expression of nonstructural protein 4 (NSP4) alone dramatically increase cytosolic calcium, which is essential for replication and assembly of infectious virions. This work identifies the intracellular mechanism by which NSP4 disrupts calcium homeostasis by showing that NSP4 is a viroporin, a class of virus-encoded transmembrane pores. Mutational analyses identified residues critical for viroporin activity. Viroporin mutants did not elevate the levels of cytoplasmic calcium in mammalian cells and were maintained in the endoplasmic reticulum rather than forming punctate vesicular structures that are critical for virus replication and morphogenesis. Pharmacological elevation of cytoplasmic calcium levels rescued puncta formation in viroporin mutants, demonstrating that elevation of calcium levels and puncta formation are distinct NSP4 functions. While viroporins typically function in virus entry or release, elevation of calcium levels by NSP4 viroporin activity may serve as a regulatory function to facilitate virus replication and assembly.**

Received 13 October 2010 **Accepted** 27 October 2010 **Published** 30 November 2010

Citation Hyser, J. M., M. Collinson-Pautz, B. Utama, and M. K. Estes. 2010. Rotavirus disrupts calcium homeostasis by NSP4 viroporin activity. mBio 1(5):e00265-10. doi:10.1128/mBio.00265-10.

Editor Terence Dermody, Vanderbilt University Medical Center

Address correspondence to Mary K. Estes, mestes@bcm.edu.

Maintenance of ion gradients across membranes is crucial for cell viability and involves the coordinated function of a myriad of channels and transporters (1). Several viruses alter intracellular ion concentrations by producing pore-forming proteins that insert into intracellular or plasma membranes to disrupt the normal electrochemical ion gradients. These viral pore-forming proteins, classified as viroporins, are found in a wide variety of DNA (2–4) and RNA virus families (5–7).

Viroporins are small, hydrophobic proteins that oligomerize to create a transmembrane aqueous pore. While viroporins target different intracellular compartments and ions, this class of proteins shares some common structural motifs, such as a hydrophobic domain that forms an amphipathic α-helix and a cluster of basic (positively charged) residues that electrostatically interact with negatively charged phospholipids to aid in membrane insertion (6). While some viroporins, such as HIV Vpu, have a single transmembrane helix, others, such as hepatitis C virus (HCV) p7, form a two-helix transmembrane hairpin (8). Viroporins fulfill a range of functions for different viruses, such as being structural proteins that facilitate virus entry (influenza M2) (9) or release (HIV Vpu, HCV p7, or polyomavirus VP4/agnoprotein) (4, 10, 11), block apoptosis (respiratory syncytial virus [RSV] SH) (12), or activate transcription factors to promote latency (human T-cell leukemia virus type 1 [HTLV-1] p12I) (13).

Chief among biologically relevant ions is calcium, a universal secondary messenger involved in most cellular processes. Calcium concentrations are strictly regulated in different cellular compartments, and viruses have developed a wide-range of strategies to

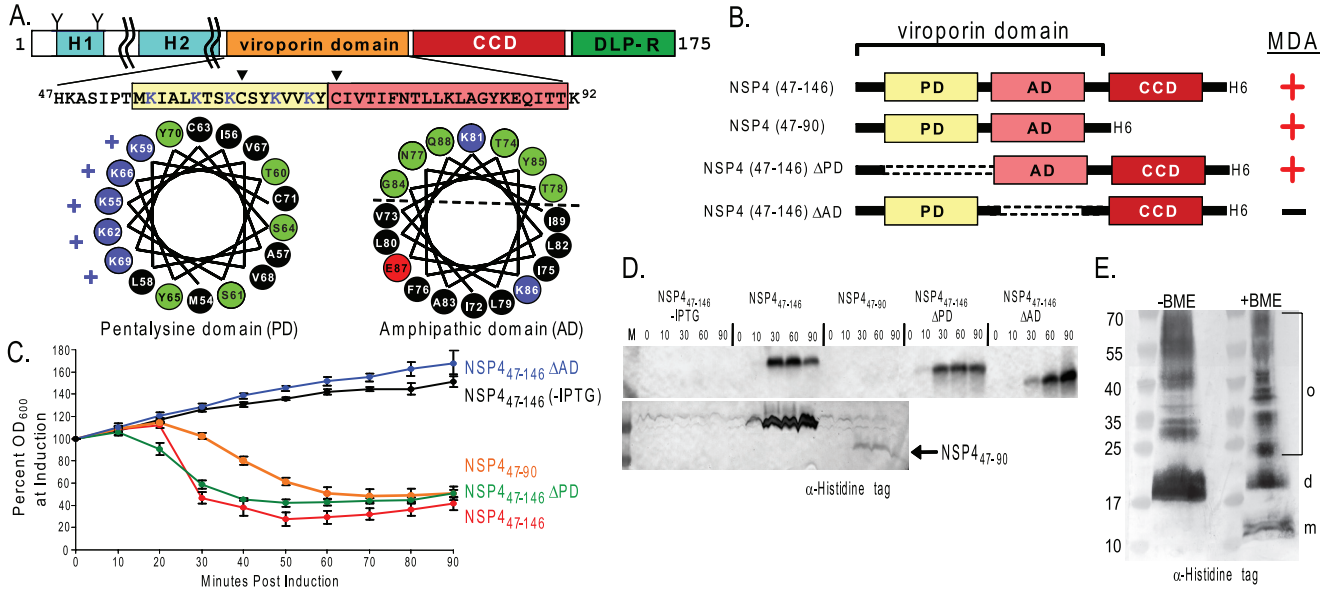

FIG 1 The amphipathic domain mediates membrane permeabilization. (A) Linear schematic of NSP4 and the primary sequence of the viroporin domain highlighting the five conserved lysines (blue) and two conserved cysteines (arrowheads). H1 and H2, hydrophobic domains 1 and 2, respectively; CCD, coiled-coil domain; DLP-R, double-layered particle receptor domain. Helical wheel representations of the pentalysine domain (PD) and amphipathic domain (AD). Black, hydrophobic residues; green, polar uncharged residues; blue, basic residues; red, acidic residues. (B) Schematic of the NSP4 deletions tested. The membrane-destabilizing activity (MDA) is summarized at the right (+, activity; −, no activity). (C) The OD_{600} of uninduced (−IPTG, black line) or NSP4-expressing cultures were determined at 10-min intervals for 90 minutes and presented as the percent optical density relative to the optical density at the time of induction. (D) Immunoblot analysis of NSP4 expression. Fivefold more lysate was loaded in the bottom immunoblot to detect $NSP4_{47-90}$. (E) Oligomerization of partially purified $NSP4_{47-90}$ was analyzed by immunoblot analysis after SDS-PAGE in the absence or presence of β-mercaptoethanol. m, monomer; d, dimer; o, oligomer.

disrupt calcium homeostasis in ways that favor virus replication, assembly, and/or release (14, 15). The best-characterized viroporins that disrupt calcium homeostasis are the enterovirus 2B proteins (16). Biochemical analysis indicates that 2B forms a transmembrane hairpin structure that inserts into the endoplasmic reticulum (ER), Golgi, and plasma membranes (17). The ability of 2B to increase levels of cytoplasmic Ca^{2+} ($[Ca^{2+}]$cyto) depends on the cationic and amphipathic nature of the pore-forming domain and is essential for virus release (18).

Rotaviruses (RV) are triple-layered nonenveloped viruses, have genomes composed of 11 segments of double-stranded RNA, and cause life-threatening viral gastroenteritis in children worldwide (19, 20). RV infection alters cellular calcium homeostasis by increasing $[Ca^{2+}]$cyto by 2- to 4-fold, increasing cellular uptake of $^{45}Ca^{2+}$ by 2-fold, depleting agonist-releasable ER calcium stores, and substantially increasing plasma membrane cation permeability (21–23). Elevated cytoplasmic and ER luminal calcium levels are crucial for virus replication and morphogenesis, since virus yields are decreased if $[Ca^{2+}]$cyto is reduced by chelating extracellular calcium with EDTA, buffering $[Ca^{2+}]$cyto with 1,2-bis(*o*-aminophenoxy)ethane-*N*,*N*,*N*′,*N*′-tetraacetic acid tetra(acetoxymethyl) ester (BAPTA-AM), blocking plasma membrane L-type calcium channels with methoxyverapamil, or blocking sarco/endoplasmic reticulum calcium ATPase (SERCA) pumps with thapsigargin (TG) (21, 22, 24, 25).

All of these changes in calcium homeostasis are recapitulated by expressing the rotavirus nonstructural protein 4 (NSP4) alone in insect and mammalian cells (26–28). NSP4 is an ER transmembrane glycoprotein that acts through a phospholipase C (PLC)-independent pathway to elevate $[Ca^{2+}]$cyto, suggesting that it may disrupt calcium homeostasis independent of the ER-associated inositol 1,4,5-trisphosphate receptor (IP3R) calcium release channel. The current studies sought to identify the domain of NSP4 that elicits the PLC-independent elevation of cytoplasmic calcium levels, to identify the mechanism by which that domain functions, and to understand whether calcium release by NSP4 regulates later steps in the RV replication cycle.

RESULTS

The NSP4 membrane-destabilizing domain has structural similarities to known viroporins. One goal of these studies was to identify the NSP4 domain that induces ER calcium permeability and the PLC-independent elevation of $[Ca^{2+}]$cyto. Previously, an ER-proximal polybasic domain (amino acids [aa] 48 to 91) was shown to permeabilize both mammalian and *Escherichia coli* membranes (29, 30). In BL21(DE3)pLysS *E. coli*, NSP4 expression disrupts inner membrane integrity, leading to T7 lysozyme-mediated cell lysis (29). Since other viroporins cause lysis in this assay (31–33), we hypothesized that this domain of NSP4 functioned as a viroporin. We analyzed NSP4 for the following structural motifs common to viroporins: oligomerization domains, lysine- or arginine-rich basic regions, and amphipathic α-helices (6, 16). Previous studies showed that NSP4 oligomerizes through a coiled-coil domain (CCD; aa 95 to 137) (34). Next, based on the helical propensity of NSP4 aa 48 to 91 ($NSP4_{48-91}$), helical wheel models of the simian agent 11 (SA11) NSP4 putative viroporin domain were generated. The N-terminal helix is predicted to be amphipathic and contains a cluster of lysine residues on one face of the helix. The C-terminal helix is also predicted to be amphipathic, with distinct polar and nonpolar surfaces (Fig. 1A). These subdomains were named the pentalysine domain (PD) and amphipathic domain (AD).

To determine if the PD, AD, and CCD were necessary for

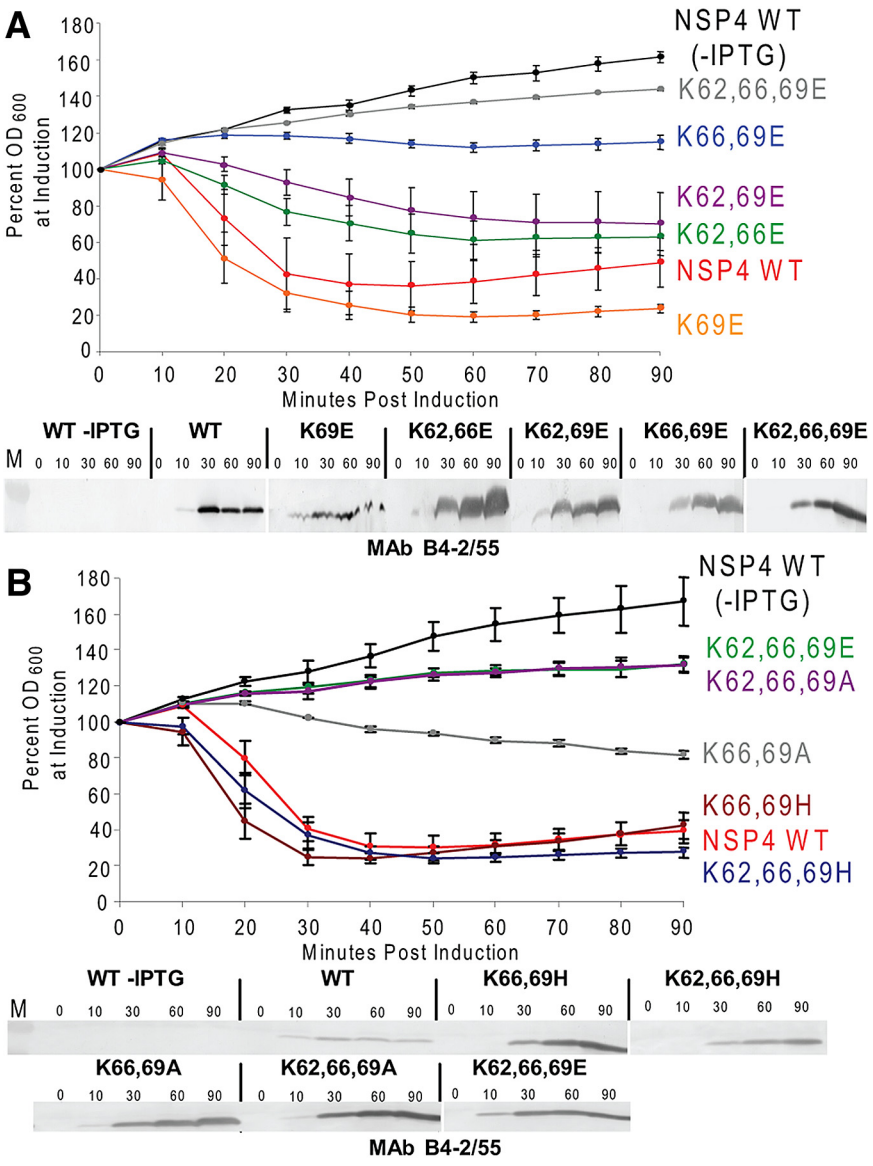

FIG 2 Positive charges of amino acids 62, 66, and 69 are crucial for NSP4 viroporin activity. (A, top) Lysine-to-glutamic acid mutants were tested in the *E. coli* lysis assay. The OD_{600} of uninduced (−IPTG, black line) or NSP4-expressing cultures was determined at 10-min intervals for 90 minutes and presented as the percent optical density relative to the optical density at the time of induction. (Bottom) Immunoblot of NSP4 expression using monoclonal antibody B4-2/55. (B, top) Lysine-to-alanine and lysine-to-histidine mutants were tested in the *E. coli* lysis assay, as described above. (Bottom) Immunoblot of NSP4 expression using monoclonal antibody B4-2/55.

membrane permeabilization, SA11 NSP4 truncation and deletion constructs were tested for membrane-destabilizing activity (MDA) using the bacterial lysis assay (Fig. 1B). In the absence of IPTG (isopropyl-β-D-thiogalactopyranoside), bacteria bearing an $NSP4_{47\text{-}146}$ expression vector continued to grow (Fig. 1C, black line), but induction of NSP4 expression led to rapid cell lysis (red line). Cell lysis was not directly caused by NSP4 because the optical density of BL21(DE3) *E. coli* (lacking lysozyme) expressing $NSP4_{47\text{-}146}$ remained stable (see Fig. S1 in the supplemental material). Expression of $NSP4_{47\text{-}90}$, which includes only the PD and AD, slowed the kinetics but not the extent of cell lysis (Fig. 1C, orange line). Deletion of the PD had no effect on MDA (Fig. 1C, blue line), but deletion of the AD abrogated lysis (green line). Immunoblot analysis showed that all four constructs were expressed, though detection of $NSP4_{47\text{-}90}$ required that 5-fold more cell lysate had to be analyzed, reflecting a lower level of expression (Fig. 1D).

The MDA of $NSP4_{47\text{-}90}$ suggested that the putative viroporin domain could oligomerize independently of the CCD. To test this, partially purified $NSP4_{47\text{-}90}$ was analyzed by immunoblotting following reducing or nonreducing sodium dodecyl sulfate-polyacrylamide gel electrophoresis (SDS-PAGE) (Fig. 1E). In the absence of β-mercaptoethanol (BME), the major species detected had the fastest-migrating band of ~18 kDa, and slower-migrating species were also detected, with their molecular masses increasing in ~12-kDa increments. In the presence of BME, the fastest-migrating band was ~10 kDa, and slower-migrating species increased in molecular masses of ~6-kDa increments. These data indicate that $NSP4_{47\text{-}90}$ forms disulfide-stabilized dimers that further oligomerize into higher-molecular-weight species that are stabilized by the lipid-mimetic SDS in the running buffer. The putative viroporin domain contains two conserved cysteine residues (Fig. 1A, arrowheads) that could support disulfide bond formation, and SDS-stabilized oligomers have been observed for other viroporins (35–37). Together, these data show that the viroporin domain oligomerizes independently of the CCD and is sufficient for NSP4 MDA and that this activity is mediated by the AD amphipathic α-helix.

PD lysine residues 62, 66, and 69 promote NSP4 MDA. The above-described results suggested that the PD is dispensable for MDA when this domain is deleted from NSP4, leaving the AD with a free amino terminus. However, clustered lysine residues are important for the activity of other viroporins (38, 39), so we next sought to determine whether the five clustered lysine residues were important for NSP4 MDA in the context of the full viroporin domain. First, using site-directed mutagenesis, all five positively charged lysine residues (aa 55, 59, 62, 66, and 69) in the SA11 $NSP4_{47\text{-}146}$ truncation were replaced by glutamic acid, a negatively charged residue that would not disrupt the helical propensity. This mutation blocked MDA, indicating that one or more lysine residues were crucial for NSP4-mediated membrane disruption (data not shown). To determine which lysine residues were important, each lysine was replaced by glutamic acid individually or in combinations of two or three within the context of SA11 $NSP4_{54\text{-}146}$. This slightly shorter construct was used to make the generation of multiple mutations easier, and no

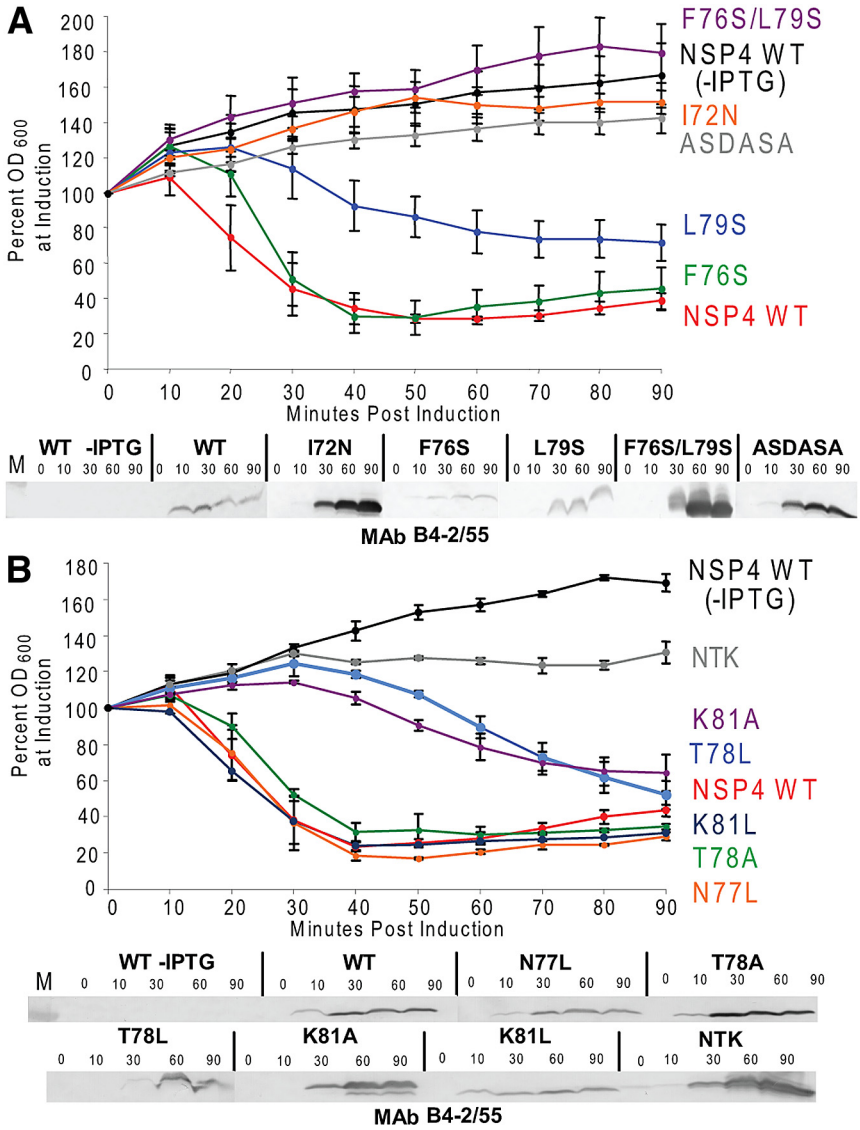

FIG 3 The amphipathic α-helix is crucial for NSP4 viroporin activity. (A) Mutations of the nonpolar surface of the amphipathic domain were tested in the *E. coli* lysis assay. (Top) The OD_{600} of uninduced (−IPTG, black line) or NSP4-expressing cultures was determined at 10-min intervals for 90 minutes and presented as the percent optical density relative to the optical density at the time of induction. (Bottom) Immunoblot of NSP4 expression using monoclonal antibody B4-2/55. (B, top) Single and multiple mutations of the polar surface of the amphipathic domain were tested in the *E. coli* lysis assay, as described above. (Bottom) Immunoblot of NSP4 expression using monoclonal antibody B4-2/55.

difference in the rate or extent of bacterial cell lysis was observed between $NSP4_{47-146}$ and $NSP4_{54-146}$ (compare red lines of Fig. 1C and 2A). The MDA of wild-type (WT) $NSP4_{54-146}$ (red line) was equivalent to that of the single lysine-to-glutamic acid mutant K69E (Fig. 2A, orange line) and the other single mutants (data not shown). Double or triple mutations of any combination of K55, K59, and K62 to glutamic acid also showed wild-type MDA (data not shown). Double or triple mutations of any combination of K62, K66, and K69 to glutamic acid (K62,66,69E) reduced $NSP4_{54-146}$ MDA (Fig. 2A), with the triple K62,66,69E mutation (gray line) showing continued growth similar to that of the uninduced negative control. Immunoblot analysis of total cell lysates showed expression of each mutant (Fig. 2A, bottom). These data indicate that the C-terminal lysine residues (aa 62, 66, and 69) within the PD were important for NSP4 MDA.

Lysine is uniquely suited for membrane interaction because the positively charged ε-amine can form an electrostatic interaction with the negatively charged phosphate head group, bringing a protein in close proximity to the membrane (40). Positively charged residues (lysine or arginine) are highly conserved within the PD among all serogroup A rotavirus NSP4 sequences (41), suggesting that the charge may be functionally relevant. To determine whether the charges of residues 62, 66, and 69 were crucial for NSP4 MDA, we constructed lysine-to-alanine (a nonpolar residue) and lysine-to-histidine (an aromatic basic residue) mutants and tested them in the bacterial lysis assay (Fig. 2B). While both the double (K66,69H) (Fig. 2B, maroon line) and triple (K62,66,69H) (blue line) lysine-to-histidine mutants showed wild-type MDA, the double lysine-to-alanine mutant (K66,69A) (Fig. 2B, gray line) showed impaired activity, and the triple lysine-to-alanine mutant (K62,66,69A) (purple line) had no MDA, similar to that of the K62,66,69E mutant (Fig. 2B). Immunoblot analysis confirmed similar expression of the constructs (Fig. 2B, bottom). These data indicate that mutations that disrupt the positive charge of the PD also disrupt NSP4 MDA.

Amphipathicity of the viroporin domain is necessary for MDA. In viroporins, the amphipathic α-helix forms the pore lumen upon oligomerization of the protein. Thus, disruption of NSP4 AD amphipathicity would be predicted to abolish MDA. To test this prediction, a six-residue mutant was constructed that changed aa 75 to 80 from IFNTLL to ASDASA and substantially decreased the amphipathic moment of the AD (see Fig. S2 in the supplemental material). As expected, the ASDASA mutant had no MDA (Fig. 3A, gray line). To identify residues on the polar and nonpolar sides of the AD crucial for MDA, we made point mutations in the context of SA11 $NSP4_{54-146}$. Residues on the nonpolar side were replaced by either serine or asparagine (small polar residues), whereas residues on the polar side were replaced by either alanine or leucine (small and large nonpolar residues). The MDA of the AD mutants clustered into the following three groups: wild-type MDA (C71S, F76S, N77A, T78A, L80S, K81L, and N77A T78A) (Fig. 3A, red line), impaired MDA (V73S, I75S, T78L, L79S, and K81A) (Fig. 3A, blue line), and no MDA (I72N, F76S L79S, N77A K81A, N77L T78L K81L, and ASDASA) (Fig. 3A, black line; see also Table S1 in the supplemental material). Single mutation of nonpolar residues I72 and L79 abolished (Fig. 3A, orange line) or impaired

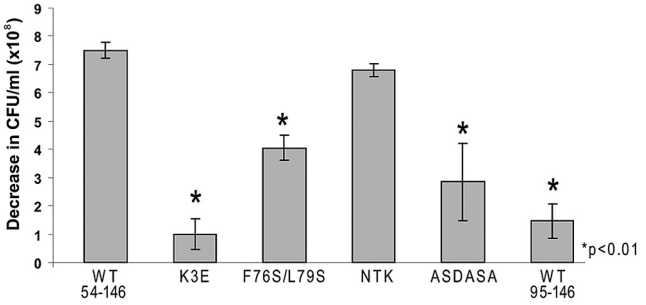

FIG 4 NSP4 cytotoxicity is mediated by the viroporin domain. Serial dilutions of the indicated constructs were plated on plates with LB-Amp and LB-Amp plus IPTG and incubated overnight at 37°C. The difference in the numbers of CFU/milliliter between LB-Amp and LB-Amp plus IPTG is graphed. *, $P < 0.01$.

(blue line) MDA. Single mutation of F76S had wild-type MDA (Fig. 3A, green line), but the F76S L79S double mutant had no MDA (Fig. 3A, purple line). Thus, the combined F76S L79S mutation exerted a synergistic blocking effect on membrane permeabilization. No single mutation of polar face residues abolished MDA. Mutants T78L (Fig. 3B, purple line) and K81A (light blue line) showed impaired activity, though protein expression of T78L was slightly delayed (Fig. 3B, bottom). Mutation K81A impaired NSP4 MDA (Fig. 3B, purple line), but mutation K81L (dark blue line) had wild-type MDA, indicating that residue choice affected the observed MDA. Finally, the triple-leucine mutation N77L T78L K81L (NTK) abolished MDA, again showing that multiple mutations have synergistic blocking effects (Fig. 3B, gray line). Together, these data indicate that the overall amphipathic nature of the AD is essential to support MDA.

The importance of α-helical secondary structure was investigated by inserting a proline-glycine dipeptide (PG) at various places within the PD or AD (see Fig. S3 in the supplemental material) within the $NSP4_{54-146}$ construct. Since PG disrupts helices, if the structure at the site of insertion is important, then the MDA would be reduced. PG insertion after lysine 59, which is not important for MDA, had wild-type MDA (see Fig. S3, orange line, in the supplemental material). PG insertion after residues 62 or 67 reduced the rate, but not the extent, of MDA (see Fig. S3, green and blue lines). PG insertion after residues 71 and 76 (within the AD) significantly impaired and abolished MDA, respectively (see Fig. S3, dark blue and gray lines, respectively). Thus, the propensity of the viroporin domain to form a helical structure is important, though to differing degrees depending on the location.

NSP4 bacterial cytotoxicity is mediated by the viroporin domain. While bacterial lysis in the above-described assays was mediated by T7 lysozyme, it remained unclear whether NSP4 was cytotoxic to cells. Since the optical density of cells lacking lysozyme upon induction of $NSP4_{47-146}$ expression remained unchanged (see Fig. S1 in the supplemental material), NSP4 expression may cause cell death in the absence of cell lysis. To determine if wild-type or mutant NSP4 proteins decreased cell viability, the number of CFU/milliliter plated in the absence or presence of 1 mM IPTG was determined (Fig. 4). Wild-type $NSP4_{95-146}$, which lacks the viroporin domain, was used as the negative control and showed a decrease of only 2×10^8 CFU/ml. In contrast, the viability of wild-type $NSP4_{54-146}$-expressing cells dropped by 7×10^8 CFU/ml, a >99% decrease. The NTK mutant had a similar drop in cell viability, but expression of the K62,66,69E, F76S L79S, and ASDASA mutants showed a significantly attenuated loss of viability. Thus, these data show that NSP4 itself is cytotoxic to bacteria without causing cell lysis, and the putative viroporin domain is the primary mediator of this cytotoxicity.

The NSP4 viroporin domain is inserted into membranes. Based upon the structure of the 2B viroporin, the NSP4 viroporin domain would be predicted to form a two-helix transmembrane hairpin. However, this predicted structure conflicts with the accepted topology of full-length NSP4, wherein aa 25 to 44 is an ER signal sequence that directs transmembrane insertion, and the viroporin domain is peripherally associated with the cytoplasmic surface of the membrane (42). Thus, we sought to determine if, in the absence of the transmembrane domain encompassing aa 25 to 44, the viroporin domain is peripherally associated with membranes, as predicted by the current topology model, or inserted through membranes, as would be expected if NSP4 is a viroporin. A series of truncations (Fig. 5A) that contain both the viroporin domain and the soluble CCD ($NSP4_{47-146}$), only the viroporin domain ($NSP4_{47-90}$), or only the CCD ($NSP4_{95-146}$), a soluble tetrameric coiled-coil domain (43), were expressed in bacteria. The cells were separated into soluble, peripheral, or integral membrane fractions and analyzed by immunoblotting (Fig. 5B). Both $NSP4_{47-146}$ and $NSP4_{47-90}$ were found solely in the integral membrane protein fraction, but $NSP4_{95-146}$ was found predominantly in the soluble fraction, indicating the viroporin domain directed membrane insertion of the $NSP4_{47-146}$ and $NSP4_{47-90}$ truncations.

To determine if the PD or AD mutants altered membrane insertion of the viroporin domain, we compared the membrane fractionation profiles of K55,59,62,66,69E and ASDASA with that of wild-type $NSP4_{47-146}$ (Fig. 5C). As before, wild-type $NSP4_{47-146}$ was found entirely in the integral membrane fraction, as was the ASDASA mutant. The K55,59,62,66,69E mutant migrated slightly faster due to a greater net negative charge and was found primarily in the peripheral membrane protein fraction, with a minor amount detected in the integral membrane fraction. Thus, while disruption of both the positive charge of the PD and the amphipathic organization of the AD blocked NSP4 MDA, only disruption of the positive charge prevented transmembrane insertion of the viroporin domain. Together, these data point to a role for the PD in membrane insertion of NSP4.

To assess whether mutations of the viroporin domain affected the expression or folding of full-length NSP4 expressed in mammalian monkey kidney cells, NSP4-enhanced green fluorescent protein (EGFP) fusion proteins for WT or K62,66,69E,NTK and ASDASA viroporin mutants were tested by immunoblotting. WT NSP4-EGFP was expressed, and endo-β-*N*-acetylglucosaminidase H (endo H) treatment, to remove N-linked carbohydrates, increased NSP4 migration, indicating that it was glycosylated (Fig. 5D). Both the NTK and ASDASA mutants were expressed and glycosylated similarly to WT NSP4 (NTK data not shown). K62,66,69E was barely detectable by immunoblotting, migrated similarly to unglycosylated NSP4, and was not susceptible to endo H treatment; however, treatment with the proteosome inhibitor MG132 (50 μM) increased levels of nonglycosylated K62,66,69E (Fig. 5D), suggesting that it might be targeted for endoplasmic reticulum-associated degradation (ERAD) (44). These data were confirmed by flow cytometry, as the mean fluorescence intensity (MFI) for K62,66,69E was significantly lower than that of the WT and increased 288% with MG132 treatment (Fig. 5E). To ensure that K62,66,69E was still membrane associated, we sepa-

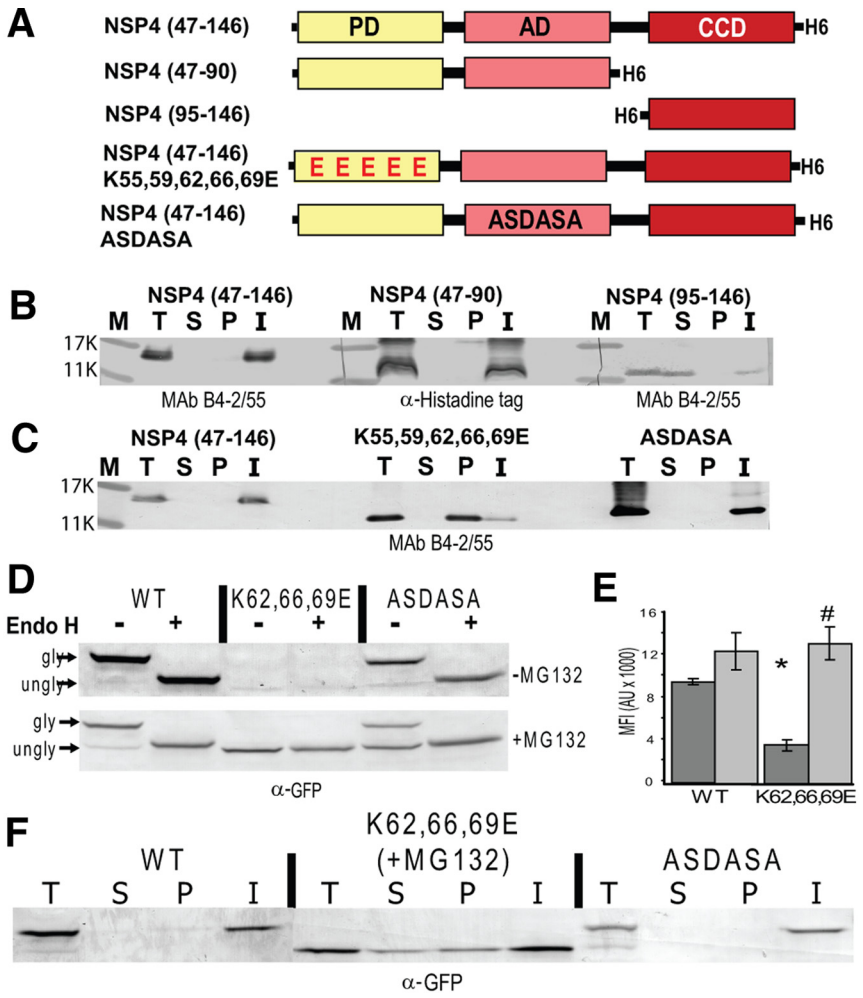

FIG 5 The pentalysine motif mediates integral membrane insertion of the viroporin domain. (A) Schematic of the NSP4 constructs tested. (B and C) Immunoblot analysis of NSP4 in total cell lysate (T), soluble protein (S), peripheral membrane protein (P), and integral membrane protein (I) fractions. M, molecular weight marker. (D) Immunoblot analysis of MA104 cell lysates for WT NSP4-EGFP, K62,66,69E, and ASDASA in the absence or presence of MG132. Lysates were mock treated or Endo H treated to demonstrate the glycosylation of NSP4 (gly) by shifting to the unglycosylated form (ungly). (E) Flow cytometry analysis of the mean fluorescence intensity (MFI) of MA104 cells expressing WT NSP4-EGFP or K62,66,69E in the absence (dark gray) or presence (light gray) of MG132. *, $P < 0.01$ for K62,66,69E versus WT in the absence of MG132; #, $P < 0.01$ for K62,66,69E absence versus the presence of MG132. AU, arbitrary units. (F) Immunoblot analysis of MA104 fractionation, as described above, for WT, K62,66,69E, and ASDASA.

rated cells into soluble, peripheral, and integral membrane fractions, marked by immunoblot detection of GFP, GM130, and STIM-1, respectively (see Fig. S4 in the supplemental material). In the absence of MG132, the WT and ASDASA were detected exclusively in the integral membrane fraction. In the presence of MG132, K62,66,69E was found primarily in the integral membrane fraction, but some protein was detected in the soluble and peripheral membrane protein fractions (Fig. 5F). Together, these data suggest that NSP4 is initially targeted to the ER membrane via the noncleaved signal sequence (aa 28 to 44), but the lysine cluster directed translocation of the viroporin domain (aa 47 to 90) into the membrane. Altering the charge of the lysine cluster blocked membrane insertion of the viroporin domain in *E. coli* and targeted NSP4 for ERAD-mediated degradation in mammalian cells. Thus, the lysines facilitate proper NSP4 folding by directing viroporin domain insertion into the membrane.

Viroporin mutants fail to elevate intracellular calcium levels in mammalian cells. Intracellular expression of full-length NSP4 in eukaryotic cells leads to increased ER permeability and a significant increase in $[Ca^{2+}]$cyto (26, 28). We tested the mutants characterized using the *E. coli* lysis assay to determine if the viroporin domain is responsible for the increased $[Ca^{2+}]$cyto using the fluorescent calcium indicator Indo-1. Using flow cytometry, we measured the mean $[Ca^{2+}]$cyto of cells expressing EGFP, the WT, or viroporin mutant NSP4-EGFP (Fig. 6). Expression of WT NSP4-EGFP increased the ratio of calcium-bound to calcium-free Indo-1 fluorescence, shifting the EGFP-positive population to the right (Fig. 6A, blue), but histograms for cells expressing NSP4-EGFP K62,66,69E or ASDASA remained clustered to the left (Fig. 6A, red and green, respectively). Cytoplasmic calcium levels (Fig. 5B) were 3.7-fold higher in cells expressing WT NSP4-EGFP (119.6 ± 33.8 nM) than in cells expressing the EGFP negative control (25.3 ± 11.3 nM). NTK viroporin mutant-expressing cells have a similar elevation in free calcium levels (111.6 ± 22.9 nM), but cells expressing the K62,66,69E or ASDASA viroporin mutants had significantly lower levels of free calcium (40.0 ± 4.0 nM and 47.4 ± 5.0 nM, respectively) than cells expressing WT NSP4-EGFP ($P < 0.05$). Together, these data show that the NSP4 viroporin domain is responsible for elevating $[Ca^{2+}]$cyto, and mutations that abrogated MDA and *E. coli* cytotoxicity correlated with the inability to elevate $[Ca^{2+}]$cyto.

NSP4 viroporin mutants are ER localized and require exogenous calcium stimulation to form vesicular puncta. Previous studies demonstrated that three pools of NSP4 exist within mammalian cells that localize to the (i) rough ER, (ii) ER-Golgi intermediate compartment (ERGIC), and (iii) puncta containing the autophagy marker LC3. NSP4 puncta formation is calcium dependent, such that NSP4 is localized to the ER if $[Ca^{2+}]$cyto remains low but an increase in the $[Ca^{2+}]$cyto causes rapid formation of the puncta, and in rotavirus-infected cells, NSP4 colocalizes with LC3 in these puncta that surround viroplasms, cytoplasmic inclusions where genome replication and progeny virus assembly occur (45). Thus, assessment of NSP4 puncta formation acts as a surrogate for testing the ability of viroporin mutants to form the viroplasm-associated puncta. The subcellular localization and distribution of WT or mutant NSP4-EGFP fusion proteins were analyzed in normal medium (1.8 mM $CaCl_2$), which supports spontaneous puncta formation for wild-type NSP4. The extent of ER localization for EGFP, WT NSP4-

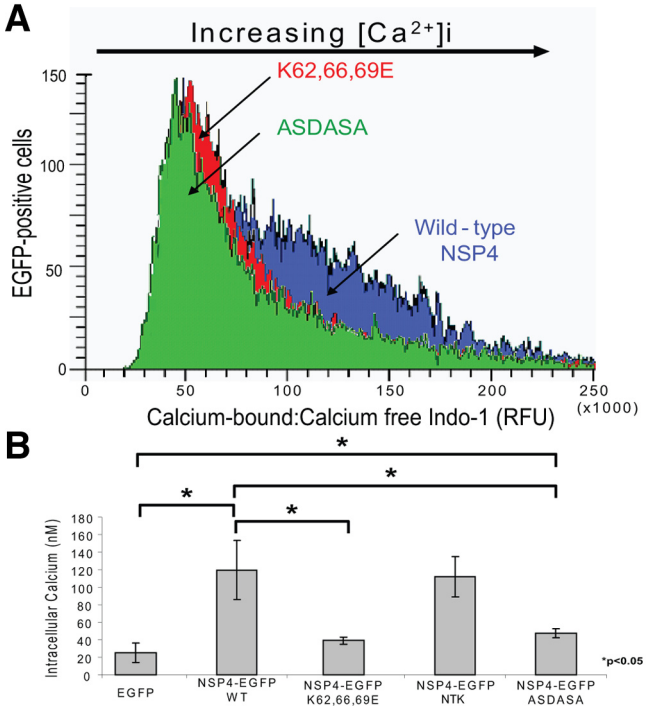

FIG 6 NSP4 viroporin mutants do not elevate cytoplasmic calcium levels. (A) HEK293T cells expressing EGFP, WT NSP4-EGFP, or the indicated viroporin mutant NSP4-EGFP were loaded with 1.8 μM Indo-1 and analyzed by flow cytometry to measure the levels of cytoplasmic calcium. RFU, relative fluorescence units. (B) The calcium-bound/calcium-free Indo-1 ratio (R) was determined for 10,000 EGFP-positive cells, and the $[Ca^{2+}]$cyto was calculated. A total of 3 independent experiments were performed, and error bars indicate the standard deviations of the means. *, $P < 0.05$.

EGFP, and the three NSP4-EGFP viroporin mutants (K62,66,69E, NTK, and ASDASA) was determined by colocalization with an ER-targeted DsRed2 fluorescent protein using confocal microscopy (Fig. 7A). EGFP was found throughout the cell and did not localize to the ER or form puncta (Fig. 7A, first row). As seen previously, WT NSP4-EGFP localized partially to the ER compartment and to distinct puncta that did not contain the DsRed-ER marker (Fig. 7A, second row). In contrast, NSP4-EGFP viroporin mutants were localized primarily in the ER, with cells expressing K62,66,69E and ASDASA lacking puncta (Fig. 7A, third and fifth rows, respectively), with a few small discrete puncta that did not contain DsRed-ER being observed in cells expressing NTK.

Next, we tested if changes in $[Ca^{2+}]$cyto directly regulated puncta formation by quantitating the number of NSP4-EGFP-expressing cells containing puncta (i) in normal DMEM, (ii) after treatment with the intracellular calcium chelator BAPTA-AM, or (iii) after treatment with TG, a SERCA pump inhibitor that elevates cytoplasmic calcium levels. This experiment was designed to determine if BAPTA treatment to buffer the elevated $[Ca^{2+}]$cyto caused by the viroporin activity of WT NSP4 would decrease puncta formation and if TG treatment to pharmacologically elevate $[Ca^{2+}]$cyto would induce puncta formation of NSP4 viroporin-deficient mutants. In normal DMEM, WT NSP4-EGFP formed discrete puncta in 93.3% of cells, but the viroporin mutants formed significantly fewer puncta, with rates of 9.4% for K62,66,69E, 55.5% for NTK, and 10.7% for ASDASA (Fig. 7B, black bars) ($P < 0.01$). BAPTA-AM treatment of WT NSP4-EGFP-expressing cells reduced puncta formation to 53.7% (Fig. 7B) ($P < 0.01$). An overall decrease in the number of puncta-containing cells was also observed in BAPTA-treated viroporin mutant-expressing cells (Fig. 7B) (P of <0.01 for NTK and ASDASA). Finally, cytoplasmic calcium levels were elevated pharmacologically with TG to determine if exogenous calcium stimulation would induce puncta formation of the viroporin NSP4-EGFP mutants. TG treatment did not significantly increase the number of puncta-containing WT NSP4-EGFP-expressing cells (Fig. 7B). In contrast, TG treatment increased puncta formation by 28.4% for K62,66,69E, 25.7% for NTK, and 39.5% for ASDASA (Fig. 7B, light gray). Thus, mutation of the viroporin domain decreased spontaneous puncta formation; however, pharmacological elevation of $[Ca^{2+}]$cyto induced puncta formation of the mutant proteins. Together, these data show (i) that the viroporin mutants were specifically deficient in the elevation of $[Ca^{2+}]$cyto but not in the ability to form puncta, (ii) that elevated $[Ca^{2+}]$cyto triggers the trafficking of NSP4 out of the ER and into cytoplasmic puncta, and (iii) that elevation of $[Ca^{2+}]$cyto and formation of puncta are separable steps within this process.

DISCUSSION

Seeking to define the mechanism for the PLC-independent increase in $[Ca^{2+}]$cyto, we investigated a previously described NSP4 domain (aa 48 to 91) with membrane-destabilizing activity that mediates cytotoxic effects in both *E. coli* and mammalian cells (29, 30). This study reports a comprehensive biochemical and mechanistic characterization of a viroporin domain from a viral nonstructural protein that alters cellular calcium homeostasis to regulate the progression of virus replication and assembly. The major new findings of this study are as follows: (i) NSP4 aa 47 to 90 were structurally similar to those of the enterovirus 2B protein and functionally consistent with the defining characteristics of viroporins, (ii) the NSP4 PD mediated integral membrane insertion of the viroporin domain, (iii) NSP4 viroporin mutants that failed to induce *E. coli* lysis and cytotoxicity also failed to elevate $[Ca^{2+}]$cyto in mammalian cells, and (iv) elevation of $[Ca^{2+}]$cyto regulates the subcellular distribution of NSP4 by triggering the movement of NSP4 out of the ER and into cytoplasmic puncta.

Using the *E. coli* lysis assay, we were able to show that the PD and AD are functionally distinct motifs within the viroporin domain. The PD functioned as a membrane insertion motif, but the PD alone did not support viroporin activity. In contrast, viroporin activity was mediated by the AD (aa 70 to 85), and mutation of this motif blocked viroporin activity but not membrane insertion. The AD also plays a role in NSP4 oligomerization by promoting the formation of high-molecular-weight NSP4 multimers that were lost by disrupting this domain (46). We confirmed this observation, since expression of the viroporin domain alone (aa 47 to 90) had viroporin activity and formed disulfide-bonded dimers and SDS-stable oligomers (Fig. 1E), which have been seen with other viroporins (35, 36). Therefore, oligomerization of the viroporin domain can occur in the absence of the CCD. Though direct evidence that this domain forms a pore is needed, this can be demonstrated only by an atomic structure of NSP4, which is hampered by the necessity to use detergent to extract NSP4 during purification.

While full-length NSP4 is targeted to the ER membrane by an uncleaved signal sequence (aa 25 to 44) (42), membrane insertion of

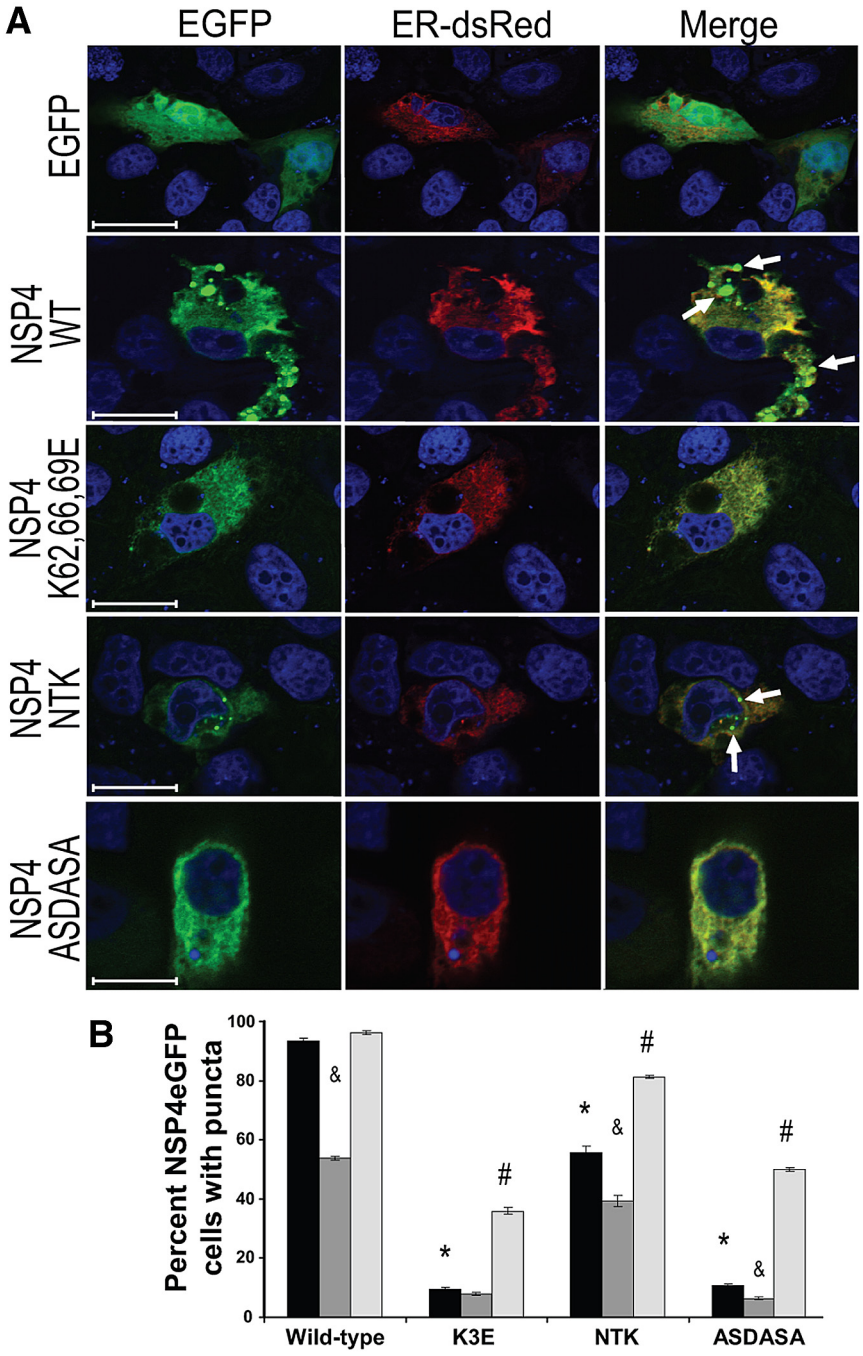

FIG 7 Mutation of the viroporin domain blocks spontaneous NSP4-EGFP puncta formation but not the ability to form puncta after Ca^{2+} stimulation. (A) Confocal microscopy images of cells expressing EGFP, WT NSP4-EGFP, or viroporin mutants (first column), the DsRed-ER marker of the endoplasmic reticulum compartment (second column), and the merged images (third column). White arrows indicate the characteristic NSP4-EGFP punctate structures. Bar = 20 μm. (B) NSP4-EGFP-expressing cells were scored for punctate or reticular EGFP signal in normal medium (black), a 50-μM BAPTA-AM treatment (dark grey), or a 1-μM TG treatment (light grey). *, $P < 0.01$ for the mutant versus the WT in normal media. &, $P < 0.01$ for the mutant in BAPTA versus in normal medium; #, $P < 0.01$ for the mutant in TG versus in normal medium.

the viroporin domain was mediated by the clustered lysine residues. These data support a new topology model for NSP4, where transmembrane insertion of the viroporin domain leads to a 3-pass transmembrane topology (Fig. 8). The NSP4 viroporin domain likely forms a two-helix hairpin, similar to that of HCV p7, because the C terminus is known to be exposed to the cytoplasmic side of the ER membrane and functions as an intracellular receptor for immature virions (8, 47). Oligomerization of NSP4 around the amphipathic α-helix would then create an aqueous channel through which Ca^{2+} could pass. This new model incorporates and is consistent with two early studies of NSP4 topology that identified either aa 25 to 44 or aa 67 to 85 as being the single transmembrane segment (42, 48).

While transmembrane translocation of the highly charged pentalysine motif seems energetically unfavorable, this phenomenon has been seen for both cationic antimicrobial peptides and other viroporins (38, 49). This was recently demonstrated through molecular modeling of an HCV p7 NMR structure, which shows that the conserved dibasic motif is embedded in the membrane, with the lysine and arginine side chains directly interacting with phosphate moieties of the lipids (50). Further, lysine and arginine have long acyl chains that can invade and displace membrane lipids by snorkeling through the lipid environment to facilitate the side chain nitrogen and head group oxygen interaction (51). Such polybasic clusters in viral proteins may constitute membrane insertion motifs.

We previously showed that NSP4 forms a novel vesicular compartment concomitantly with increased $[Ca^{2+}]$cyto (45) and that these structures associate with the autophagy protein LC3 and surround viroplasms, cytoplasmic inclusions in rotavirus-infected cells that support virus replication. The formation of these vesicular puncta by exogenous expression of NSP4 serves as a surrogate for the formation of viroplasm-associated puncta. In these studies, mutation of the viroporin domain prevented the elevation of cytoplasmic Ca^{2+} levels, which correlated with the disruption of viroporin activity and loss of *E. coli* cytotoxicity. While the NTK mutant did not induce lysozyme-mediated cell lysis, it showed *E. coli* cytotoxicity and elevation of calcium levels similar to those of WT NSP4, indicating that MDA can be retained in the absence of cell lysis. The use of flow cytometry and Indo-1 as a Ca^{2+} indicator allowed single-cell analysis of a much larger population of NSP4-expressing cells than in previous studies that used single-cell microscopy and

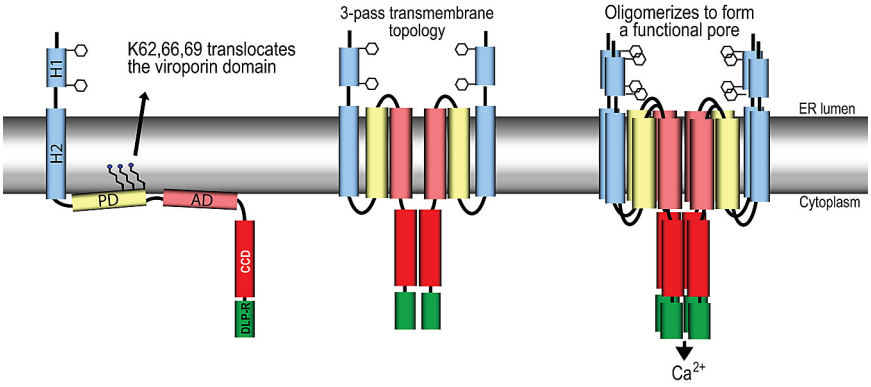

FIG 8 Model of the NSP4 viroporin as a three-pass transmembrane protein. (Left) Initial insertion of NSP4 into the ER membrane (gray) occurs through the uncleaved signal sequence in the H2 domain. Lysine residues interact with ER membrane phospholipids and promote insertion of the viroporin domain as an anti-parallel α-helical hairpin. (Center) Insertion of the viroporin domain generates a three-pass transmembrane topology. (Right) Oligomerization of NSP4 around the amphipathic α-helix creates an aqueous pore through the membrane and allows the release of ER Ca^{2+}.

Fura-2 (27, 28). Additionally, Indo-1 is less sensitive to compartmentalization into Ca^{2+}-storage organelles, allowing more accurate measurements of $[Ca^{2+}]$cyto (52).

NSP4 viroporin activity could trigger the elevation of cytoplasmic Ca^{2+} levels in several ways that are not necessarily mutually exclusive. In the ER, progressive depletion of the ER Ca^{2+} stores by ER-associated NSP4 could activate store-operated Ca^{2+} entry (SOCE) and indirectly increase plasma membrane permeability by opening cellular Ca^{2+} entry channels (26, 53). Additionally, expression of NSP4 increases plasma membrane permeability to mono- and divalent cations (28). Since NSP4 traffics to the plasma membrane in RV-infected cells, it is possible that NSP4 viroporin activity could directly increase plasma membrane permeability to Ca^{2+} and possibly other ions (28, 54). Both mechanisms rely on NSP4 viroporin activity; however, a detailed analysis of how NSP4 affects Ca^{2+} at both the ER and plasma membrane will be necessary to determine the relative importance that either direct permeabilization or SOCE activation, or both, has on the elevation of intracellular Ca^{2+} levels during a rotavirus infection.

Previous studies suggested that the movement of NSP4 from the ER into the punctate NSP4/LC3 vesicles was regulated by $[Ca^{2+}]$cyto, but since the mechanism of NSP4-mediated ER calcium release was unknown, the dependence on calcium for this process could not be characterized further (45). We demonstrated that failure of the viroporin mutants to spontaneously form puncta was a direct consequence of their inability to elevate cytoplasmic Ca^{2+} levels by measuring puncta formation after buffering (BAPTA-AM) or elevating (TG) $[Ca^{2+}]$cyto. Under normal conditions, puncta formation by NSP4 occurs spontaneously and rapidly; however, mutants of either the pentalysine domain (K62,66,69E) or amphipathic domain (ASDASA) were unable to form puncta. TG stimulation of viroporin mutant NSP4 puncta formation demonstrated that the mutations specifically blocked the elevation of $[Ca^{2+}]$cyto but not the ability to form puncta. Thus, disruption of cellular Ca^{2+} homeostasis and puncta formation are separable events, and NSP4 not only increases $[Ca^{2+}]$cyto by viroporin activity but also appears to be a sensor for changes in $[Ca^{2+}]$cyto. The NSP4 viroporin mutants developed in these studies will be useful tools to determine the precise $[Ca^{2+}]$cyto that triggers NSP4 puncta formation.

These studies demonstrate that NSP4 viroporin activity is responsible for the elevation of $[Ca^{2+}]$cyto in rotavirus-infected cells, which was first reported nearly 20 years ago (21), and appears to regulate several changes in the subcellular distribution of other RV proteins. First, elevation of cytoplasmic Ca^{2+} levels regulates the formation of viroplasms, the RV replication complex. Nonstructural protein 5 (NSP5), a component of viroplasms, has two pseudo-EF-hand Ca^{2+} binding sites and elevated levels of cytoplasmic Ca^{2+}, and Ca^{2+} binding triggers the aggregation of soluble NSP5 into a viroplasm-like structure (55). Second, in response to elevated levels of Ca^{2+}, NSP4 traffics out of the ER and into puncta that surround viroplasms. Third, the assembly of the RV outer capsid protein VP7 onto virions requires high Ca^{2+} levels inside the ER (24). Since RNA interference (RNAi)-mediated knockdown of NSP4 prevents the proper assembly of viroplasms and causes the mislocalization of several other RV proteins (56, 57), it appears that NSP4 viroporin activity functionally regulates the progression of RV infection and assembly by altering the cytoplasmic Ca^{2+} levels.

The regulatory function fulfilled by NSP4 viroporin activity is unique among viroporins, which function primarily in virus entry (influenza M2) (9), virus release (HCV p7, HIV Vpu, coronavirus E, and polyomavirus VP4/agnoprotein) (3, 10, 11, 58), or apoptosis (RSV SH) (12). While picornavirus 2B elevates Ca^{2+} levels in infected cells, the role that elevated Ca^{2+} levels plays in the replication cycle for these viruses is not well characterized (39). Thus, as is shown here for rotavirus NSP4, it is possible that the use of viroporins to modulate processes important for replication complex assembly, genome replication, and virus assembly is a mechanism utilized by more viruses than is currently appreciated.

MATERIALS AND METHODS

Expression vectors. *E. coli* expression constructs were generated by ligation-independent cloning (LIC) using the pET46Ek/LIC system (EMD Biosciences, San Diego, CA). Wild-type NSP4-EGFP was constructed by inserting the SA11 NSP4 (GenBank accession no. AF087678.1) coding region into pEGFP-N1 (Clontech). Internal deletions and mutations were generated by using the QuikChange mutagenesis kit (Stratagene, La Jolla, CA) or encoding the desired mutation in the forward primer, and all constructs were sequenced (Lone Star Laboratories, Houston, TX).

***E. coli* lysis assay.** Assessment of NSP4 viroporin activity in *E. coli* was performed essentially as described previously (31). Overnight cultures were diluted 1:100 into fresh LB and grown until the optical density at 600 nm (OD_{600}) was 0.4 to 0.6, and 1 mM IPTG was added to induce protein expression. OD_{600} measurements of each culture were taken before IPTG induction and at 10-min intervals postinduction for 90 min using a multiwell plate spectrophotometer.

Immunoblot analysis. Samples were mixed with sample buffer, boiled for 5 minutes, run on 4 to 20% Tris-glycine or 10 to 20% Tris-Tricine polyacryamide gradient gels (Bio-Rad, Hercules, CA), and transferred onto a nitrocellulose membrane (GE Healthcare Bio-Sciences Corporation, Piscataway, NJ) as previously described (59). Bacterially expressed $NSP4_{47-90}$–His was partially purified using Ni^{2+}-nitrilotriacetic acid (NTA) beads (GE Healthcare Bio-Sciences) as previously described (59) and separated by SDS-PAGE as described above, except sample

buffer lacking BME was used under nonreducing conditions. Antibodies used were NSP4 MAb B4-2/55 ascites, anti-Penta-His antibody (Qiagen, Valencia, CA), anti-EGFP monoclonal antibody (Clontech), anti-GM130 monoclonal antibody (BD Transduction Laboratories, San Jose, CA), and anti-STIM- 1 antibody (Sigma-Aldrich, St. Louis, MO).

***E. coli* viability assay.** Stationary-phase cultures of *E. coli* BL21(DE3) for the indicated NSP4 constructs were serially diluted in LB (without ampicillin), and 100 μl of each dilution was plated on LB-ampicillin plates in the absence or presence of 1 mM IPTG. The plates were incubated overnight at 37°C, and the number of CFU per milliliter was calculated.

Membrane protein fractionation. BL21(DE3)pLysS broth cultures were grown to an OD_{600} of 0.5 to 0.6, and protein expression was induced with 1 mM IPTG and cultured for 1 h. The cells were pelleted by centrifugation (21,000 × *g*, 1 h) and resuspended in 5 ml ice-cold phosphate-buffered saline (PBS) (total protein lysate fraction [T]). A 1-ml aliquot was sonicated in PBS using a probe sonicator (soluble protein fraction [S]). The membranes were pelleted by centrifugation (100,000 × *g*, 1 h) and resuspended in 1 ml 100 mM sodium carbonate for 30 min on ice (peripheral membrane protein fraction [P]). The membranes were again pelleted and resuspended in 1 ml 1% SDS-PBS (integral membrane protein fraction [I]). Equal buffer volumes were used to maintain the same relative protein concentration as that of the starting material. Equivalent amounts of each fraction were analyzed by SDS-PAGE.

Cells and transfection. African green monkey MA104 kidney cells and human embryonic kidney (HEK) 293T cells were maintained and transfected as previously described (45). In experiments using *N*-(benzyloxycarbonyl) leucinylleucinylleucinal-*Z*-Leu-Leu-Leu-al (MG132), at 4 h posttransfection, the medium was replaced with fresh Opti-MEM containing 50 μM MG132. In all cases, cells were incubated overnight at 37°C.

Confocal microscopy. MA104 cells were fixed with 4% paraformaldehyde and permeabilized with 0.5% Triton X-100 for 10 min. Cells were stained with TO-PRO-3 (Invitrogen), and coverslips were mounted onto slides using ProLong gold antifade reagents (Molecular Probes, Eugene, OR). Mounted slides were observed using a Carl Zeiss LSM 510 Meta confocal microscope with a 63× immersion oil objective (Carl Zeiss, Germany). The pinhole was set to 1, and pixel time was set at 3.20 μs for 16 scanning averages per track on each slice, and Z-stack slices were set to 1 μm. The collected images were processed using LSM 510 image software (Carl Zeiss, Inc., Thornwood, NY).

Indo-1 calcium measurements. Indo-1 (50 μg; Molecular Probes) was resuspended in 50 μl 20% F-127 and 50 μl fetal bovine serum (FBS) at 37°C. The Indo-1 loading buffer used was Hanks' balanced salt solution (HBSS; Invitrogen) supplemented with 1% bovine serum albumin (BSA) (HBSS-BSA) and 1.8 μM Indo-1. At approximately 28 h posttransfection, the cells were gently washed with HBSS-BSA, and Indo- 1 loading buffer was added for 30 min at 37°C. Cells were pelleted, resuspended in alpha-MEM (no phenol red) plus 10% FBS plus 10 mM HEPES, and maintained at 37°C until analyzed. Flow cytometry analysis was performed using an LSRII system running FACSDiva software (BD Biosciences, Franklin Lakes, NJ). Indo-1 fluorescence was excited by a UV laser (355 nm), and Ca^{2+}-free and Ca^{2+}-bound emissions were split using a 505LP dichroic filter. Ca^{2+}-free emission was collected with a 525/50-nm band-pass filter, and the Ca^{2+}-bound emission was collected with a 405/20-nm band-pass filter. EGFP fluorescence was excited by the argon laser (488 nm), and emission was collected with a 520/20-nm band-pass filter. The mean bound Ca^{2+}-to-free Ca^{2+} fluorescence ratio (R) was determined for each sample. The concentration of calcium was calculated by using the following equation: Ca^{2+} (nM) $= K_d(R - R_{min})S_{f2}/(R_{max} - R)S_{b2}$. Treatment of cells with 10 mM EDTA and 5 μM ionomycin was used to determine the fluorescence ratios at zero (R_{min}) and saturated (R_{max}) calcium, respectively. S_{f2} and S_{b2} are the fluorescence intensities of the calcium-free and -bound dyes, respectively. The dissociation constant of Indo-1 is 250 nM. Experiments were performed in triplicate, and results are presented at the mean calculated calcium level.

Puncta formation assay. MA104 cells were either loaded with 50 μM BAPTA-AM for 1 h at 37°C at 4 h posttransfection or maintained in normal medium. At approximately 20 h posttransfection, a subset of the transfected cells were treated with 1 μM thapsigargin (TG) for 3 h, and then, all the cells were fixed in 4% paraformaldehyde. The number of NSP4-EGFP-expressing cells containing diffuse rather than punctate NSP4-EGFP was counted in 25 random fields per well using the 40× lens objective on an Olympus IX70 inverted epifluorescence microscope. Cells with a completely uniform reticular NSP4-EGFP distribution were scored as having no puncta; however, cells with the presence of even one punctate structure were scored as having puncta.

Statistical analysis. Statistical differences between groups were determined using a two-tailed Student's *t* test. *P* values of <0.05 were considered significant.

ACKNOWLEDGMENTS

This work was supported in part by NIH grant R01AI080656, NIH Research Training in Pediatric Gastroenterology grant T32DK007664, an NIH Training Grant in Molecular Virology, T32AI007471, and Public Health Service grant P30DK56338, which funds the Texas Medical Center Digestive Diseases Center.

Scoring of cells was performed by J.M.H., and categorization of cells into groups with puncta/no puncta was validated by M.C.-P. and B.U.

SUPPLEMENTAL MATERIAL

Supplemental material for this article may be found at http://mbio.asm.org/lookup/suppl/doi:10.1128/mBio.00265-10/-/DCSupplemental.

Figure S1, TIF file, 3.902 MB.
Figure S2, TIF file, 5.443 MB.
Figure S3, TIF file, 5.300 MB.
Figure S4, TIF file, 3.468 MB.
Table S1, PDF file, 0.098 MB.

REFERENCES

1. **Dubyak, G. R.** 2004. Ion homeostasis, channels, and transporters: an update on cellular mechanisms. Adv. Physiol. Educ. **28**:143–154.
2. **Kang, M., A. Moroni, S. Gazzarrini, D. DiFrancesco, G. Thiel, M. Severino, and J. L. Van Etten.** 2004. Small potassium ion channel proteins encoded by chlorella viruses. Proc. Natl. Acad. Sci. U. S. A. **101**: 5318–5324.
3. **Daniels, R., D. Sadowicz, and D. N. Hebert.** 2007. A very late viral protein triggers the lytic release of SV40. PLoS Pathog. **3**:e98.
4. **Suzuki, T., Y. Orba, Y. Okada, Y. Sunden, T. Kimura, S. Tanaka, K. Nagashima, W. W. Hall, and H. Sawa.** 2010. The human polyoma JC virus agnoprotein acts as a viroporin. PLoS Pathog. **6**:e1000801.
5. **Liao, Y., J. P. Tam, and D. X. Liu.** 2006. Viroporin activity of SARS-CoV E protein. Adv. Exp. Med. Biol. **581**:199–202.
6. **Gonzalez, M. E., and L. Carrasco.** 2003. Viroporins. FEBS Lett. **552**:28–34.
7. **Perez, M., B. Garcia-Barreno, J. A. Melero, L. Carrasco, and R. Guinea.** 1997. Membrane permeability changes induced in *Escherichia coli* by the SH protein of human respiratory syncytial virus. Virology **235**:342–351.
8. **Cook, G. A., H. Zhang, S. H. Park, Y. Wang, and S. J. Opella.** Comparative NMR studies demonstrate profound differences between two viroporins: p7 of HCV and Vpu of HIV-1. Biochim. Biophys. Acta, in press.
9. **Pielak, R. M., and J. J. Chou.** Influenza M2 proton channels. Biochim. Biophys. Acta, in press.
10. **Ruiz, A., J. C. Guatelli, and E. B. Stephens.** 2010. The Vpu protein: new concepts in virus release and CD4 down-modulation. Curr. HIV Res. **8**:240–252.
11. **Steinmann, E., F. Penin, S. Kallis, A. H. Patel, R. Bartenschlager, and T. Pietschmann.** 2007. Hepatitis C virus p7 protein is crucial for assembly and release of infectious virions. PLoS Pathog. **3**:e103.
12. **Fuentes, S., K. C. Tran, P. Luthra, M. N. Teng, and B. He.** 2007. Function of the respiratory syncytial virus small hydrophobic protein. J. Virol. **81**:8361–8366.
13. **Ding, W., B. Albrecht, R. E. Kelley, N. Muthusamy, S. J. Kim, R. A. Altschuld, and M. D. Lairmore.** 2002. Human T-cell lymphotropic virus type 1 p12(I) expression increases cytoplasmic calcium to enhance the activation of nuclear factor of activated T cells. J. Virol. **76**:10374–10382.

14. **Zhou, Y., T. K. Frey, and J. J. Yang.** 2009. Viral calciomics: interplays between Ca^{2+} and virus. Cell Calcium **46**:1–17.
15. **Chami, M., B. Oules, and P. Paterlini-Brechot.** 2006. Cytobiological consequences of calcium-signaling alterations induced by human viral proteins. Biochim. Biophys. Acta **1763**:1344–1362.
16. **van Kuppeveld, F. J., A. S. de Jong, W. J. Melchers, and P. H. Willems.** 2005. Enterovirus protein 2B po(u)res out the calcium: a viral strategy to survive? Trends Microbiol. **13**:41–44.
17. **Sanchez-Martinez, S., N. Huarte, R. Maeso, V. Madan, L. Carrasco, and J. L. Nieva.** 2008. Functional and structural characterization of 2B viroporin membranolytic domains. Biochemistry **47**:10731–10739.
18. **van Kuppeveld, F. J., J. M. Galama, J. Zoll, P. J. van den Hurk, and W. J. Melchers.** 1996. Coxsackie B3 virus protein 2B contains cationic amphipathic helix that is required for viral RNA replication. J. Virol. **70**:3876–3886.
19. **Hyser, J. M., and M. K. Estes.** 2009. Rotavirus vaccines and pathogenesis: 2008. Curr. Opin. Gastroenterol. **25**:36–43.
20. **Jiang, V., B. Jiang, J. Tate, U. D. Parashar, and M. M. Patel.** Performance of rotavirus vaccines in developed and developing countries. Hum. Vaccin., in press.
21. **Michelangeli, F., M. C. Ruiz, J. R. del Castillo, J. E. Ludert, and F. Liprandi.** 1991. Effect of rotavirus infection on intracellular calcium homeostasis in cultured cells. Virology **181**:520–527.
22. **Perez, J. F., M. E. Chemello, F. Liprandi, M. C. Ruiz, and F. Michelangeli.** 1998. Oncosis in MA104 cells is induced by rotavirus infection through an increase in intracellular Ca^{2+} concentration. Virology **252**:17–27.
23. **Zambrano, J. L., Y. Diaz, F. Pena, E. Vizzi, M. C. Ruiz, F. Michelangeli, F. Liprandi, and J. E. Ludert.** 2008. Silencing of rotavirus NSP4 or VP7 expression reduces alterations in Ca^{2+} homeostasis induced by infection of cultured cells. J. Virol. **82**:5815–5824.
24. **Ruiz, M. C., O. C. Aristimuno, Y. Diaz, F. Pena, M. E. Chemello, H. Rojas, J. E. Ludert, and F. Michelangeli.** 2007. Intracellular disassembly of infectious rotavirus particles by depletion of Ca^{2+} sequestered in the endoplasmic reticulum at the end of virus cycle. Virus Res. **130**:140–150.
25. **Michelangeli, F., F. Liprandi, M. E. Chemello, M. Ciarlet, and M. C. Ruiz.** 1995. Selective depletion of stored calcium by thapsigargin blocks rotavirus maturation but not the cytopathic effect. J. Virol. **69**:3838–3847.
26. **Tian, P., M. K. Estes, Y. Hu, J. M. Ball, C. Q. Zeng, and W. P. Schilling.** 1995. The rotavirus nonstructural glycoprotein NSP4 mobilizes Ca^{2+} from the endoplasmic reticulum. J. Virol. **69**:5763–5772.
27. **Berkova, Z., A. P. Morris, and M. K. Estes.** 2003. Cytoplasmic calcium measurement in rotavirus enterotoxin-enhanced green fluorescent protein (NSP4-EGFP) expressing cells loaded with Fura-2. Cell Calcium **34**:55–68.
28. **Diaz, Y., M. E. Chemello, F. Pena, O. C. Aristimuno, J. L. Zambrano, H. Rojas, F. Bartoli, L. Salazar, S. Chwetzoff, C. Sapin, G. Trugnan, F. Michelangeli, and M. C. Ruiz.** 2008. Expression of nonstructural rotavirus protein NSP4 mimics Ca^{2+} homeostasis changes induced by rotavirus infection in cultured cells. J. Virol. **82**:11331–11343.
29. **Browne, E. P., A. R. Bellamy, and J. A. Taylor.** 2000. Membrane-destabilizing activity of rotavirus NSP4 is mediated by a membrane-proximal amphipathic domain. J. Gen. Virol. **81**:1955–1959.
30. **Newton, K., J. C. Meyer, A. R. Bellamy, and J. A. Taylor.** 1997. Rotavirus nonstructural glycoprotein NSP4 alters plasma membrane permeability in mammalian cells. J. Virol. **71**:9458–9465.
31. **Lama, J., and L. Carrasco.** 1992. Expression of poliovirus nonstructural proteins in *Escherichia coli* cells. Modification of membrane permeability induced by 2B and 3A. J. Biol. Chem. **267**:15932–15937.
32. **Gonzalez, M. E., and L. Carrasco.** 1998. The human immunodeficiency virus type 1 Vpu protein enhances membrane permeability. Biochemistry **37**:13710–13719.
33. **Guinea, R., and L. Carrasco.** 1994. Influenza virus M2 protein modifies membrane permeability in *E. coli* cells. FEBS Lett. **343**:242–246.
34. **Bowman, G. D., I. M. Nodelman, O. Levy, S. L. Lin, P. Tian, T. J. Zamb, S. A. Udem, B. Venkataraghavan, and C. E. Schutt.** 2000. Crystal structure of the oligomerization domain of NSP4 from rotavirus reveals a core metal-binding site. J. Mol. Biol. **304**:861–871.
35. **Agirre, A., M. Lorizate, S. Nir, and J. L. Nieva.** 2008. Poliovirus 2b insertion into lipid monolayers and pore formation in vesicles modulated by anionic phospholipids. Biochim. Biophys. Acta **1778**:2621–2626.
36. **Perez-Berna, A. J., J. Guillen, M. R. Moreno, A. Bernabeu, G. Pabst, P. Laggner, and J. Villalain.** 2008. Identification of the membrane-active regions of hepatitis C virus p7 protein: biophysical characterization of the loop region. J. Biol. Chem. **283**:8089–8101.
37. **Carter, S. D., K. C. Dent, E. Atkins, T. L. Foster, M. Verow, P. Gorny, M. Harris, J. A. Hiscox, N. A. Ranson, S. Griffin, and J. N. Barr.** 2010. Direct visualization of the small hydrophobic protein of human respiratory syncytial virus reveals the structural basis for membrane permeability. FEBS Lett. **584**:2786–2790.
38. **StGelais, C., T. L. Foster, M. Verow, E. Atkins, C. W. Fishwick, D. Rowlands, M. Harris, and S. Griffin.** 2009. Determinants of hepatitis C virus p7 ion channel function and drug sensitivity identified in vitro. J. Virol. **83**:7970–7981.
39. **van Kuppeveld, F. J., J. G. Hoenderop, R. L. Smeets, P. H. Willems, H. B. Dijkman, J. M. Galama, and W. J. Melchers.** 1997. Coxsackievirus protein 2B modifies endoplasmic reticulum membrane and plasma membrane permeability and facilitates virus release. EMBO J. **16**:3519–3532.
40. **Epand, R. M., and W. Lim.** 1995. Mechanism of liposome destabilization by polycationic amino acids. Biosci. Rep. **15**:151–160.
41. **Lin, S. L., and P. Tian.** 2003. Detailed computational analysis of a comprehensive set of group A rotavirus NSP4 proteins. Virus Genes **26**:271–282.
42. **Bergmann, C. C., D. Maass, M. S. Poruchynsky, P. H. Atkinson, and A. R. Bellamy.** 1989. Topology of the non-structural rotavirus receptor glycoprotein NS28 in the rough endoplasmic reticulum. EMBO J. **8**:1695–1703.
43. **Deepa, R., R. C. Durga, and K. Suguna.** 2007. Structure of the extended diarrhea-inducing domain of rotavirus enterotoxigenic protein NSP4. Arch. Virol. **152**:847–859.
44. **Vembar, S. S., and J. L. Brodsky.** 2008. One step at a time: endoplasmic reticulum-associated degradation. Nat. Rev. Mol. Cell Biol. **9**:944–957.
45. **Berkova, Z., S. E. Crawford, G. Trugnan, T. Yoshimori, A. P. Morris, and M. K. Estes.** 2006. Rotavirus NSP4 induces a novel vesicular compartment regulated by calcium and associated with viroplasms. J. Virol. **80**:6061–6071.
46. **Jagannath, M. R., M. M. Kesavulu, R. Deepa, P. N. Sastri, S. S. Kumar, K. Suguna, and C. D. Rao.** 2006. N- and C-terminal cooperation in rotavirus enterotoxin: novel mechanism of modulation of the properties of a multifunctional protein by a structurally and functionally overlapping conformational domain. J. Virol. **80**:412–425.
47. **Au, K. S., W. K. Chan, J. W. Burns, and M. K. Estes.** 1989. Receptor activity of rotavirus nonstructural glycoprotein NS28. J. Virol. **63**:4553–4562.
48. **Chan, W. K., K. S. Au, and M. K. Estes.** 1988. Topography of the simian rotavirus nonstructural glycoprotein (NS28) in the endoplasmic reticulum membrane. Virology **164**:435–442.
49. **Zakharov, S. D., T. I. Rokitskaya, V. L. Shapovalov, Y. N. Antonenko, and W. A. Cramer.** 2002. Tuning the membrane surface potential for efficient toxin import. Proc. Natl. Acad. Sci. U. S. A. **99**:8654–8659.
50. **Montserret, R., N. Saint, C. Vanbelle, A. G. Salvay, J. P. Simorre, C. Ebel, N. Sapay, J. G. Renisio, A. Bockmann, E. Steinmann, T. Pietschmann, J. Dubuisson, C. Chipot, and F. Penin.** 2010. NMR structure and ion channel activity of the p7 protein from hepatitis C virus. J. Biol. Chem. **285**:31446–31461.
51. **Kandasamy, S. K., and R. G. Larson.** 2006. Molecular dynamics simulations of model trans-membrane peptides in lipid bilayers: a systematic investigation of hydrophobic mismatch. Biophys. J. **90**:2326–2343.
52. **Wahl, M., M. J. Lucherini, and E. Gruenstein.** 1990. Intracellular Ca^{2+} measurement with Indo-1 in substrate-attached cells: advantages and special considerations. Cell Calcium **11**:487–500.
53. **Cahalan, M. D.** 2009. STIMulating store-operated Ca(2+) entry. Nat. Cell Biol. **11**:669–677.
54. **Ruiz, M. C., Y. Diaz, F. Pena, O. C. Aristimuno, M. E. Chemello, and F. Michelangeli.** 2005. Ca^{2+} permeability of the plasma membrane induced by rotavirus infection in cultured cells is inhibited by tunicamycin and brefeldin A. Virology **333**:54–65.
55. **Sen, A., N. Sen, and E. R. Mackow.** 2007. The formation of viroplasm-like structures by the rotavirus NSP5 protein is calcium regulated and directed by a C-terminal helical domain. J. Virol. **81**:11758–11767.
56. **Silvestri, L. S., M. A. Tortorici, R. Vasquez-Del Carpio, and J. T. Patton.** 2005. Rotavirus glycoprotein NSP4 is a modulator of viral transcription in the infected cell. J. Virol. **79**:15165–15174.
57. **Lopez, T., M. Camacho, M. Zayas, R. Najera, R. Sanchez, C. F. Arias, and S. Lopez.** 2005. Silencing the morphogenesis of rotavirus. J. Virol. **79**:184–192.
58. **Ye, Y., and B. G. Hogue.** 2007. Role of the coronavirus E viroporin protein transmembrane domain in virus assembly. J. Virol. **81**:3597–3607.
59. **Hyser, J. M., C. Q. Zeng, Z. Beharry, T. Palzkill, and M. K. Estes.** 2008. Epitope mapping and use of epitope-specific antisera to characterize the VP5* binding site in rotavirus SA11 NSP4. Virology **373**:211–228.